Novel modeling technique that adopts radial force generated in mixed pole generators

A. L. Mohamadein, R. A. Hamdy and Ayman S. Abdel-khalik
Electrical Eng. Dept., Faculty of Eng., Alexandria University, Alexandria, Egypt

This paper presents theoretical, simulation and experimental study of the Mixed Pole Machine (MPM), operating in the generation mode, based on a novel modeling technique. The proposed modeling technique uses the machine magnetic circuit. The paper also presents the simulation results of the radial force exerted on the rotor when the machine operates under concentric as well as eccentric rotor conditions. The operation of MPM machine with eccentric rotor positions creates asymmetrical air gap flux distributions and results in unbalanced magnetic pull. This paper presents the effect of this asymmetrical air gap flux on the resulting radial force under different conditions.

تعرض هذه المقالة الدراسة النظرية و العملية للماكينات ذات الأقطاب المختلطة والتى تعمل كمولدات باستخدام طريقة جديدة للمحاكاة. وتعتمد هذه الطريقة على الدائرة المغناطيسية لتمثيل الماكينة. كذلك تتعرض المقالة لدراسة القوى القطرية المؤثرة فى حالتى الأعضاء الدوارة المتمركزة واللامتمركزة. حيث يتسبب عدم التمركز فى عدم تماثل توزيع الفيض المغناطيسى داخل الثغرة الهوائية مما يؤدى بدوره إلى عدم اتزان القوى القطرية. وتقدم المقالة دراسة لتأثير هذا اللاتماثل فى توزيع الفيض المغناطيسى على القوى القطرية الناشئة تحت ظروف مختلفة.

Keywords: Mixed pole machine, Magnetic circuit, Skewing effect, Radial force

1. Introduction

The idea of Mixed-Pole Machine (MPM) is to have two electrically connected and mechanically coupled machines in the same frame [1]. The resulting new machine has combined characteristics from both machines.

The idea was firstly introduced from the so called “tandem connection” where two three-phase wound rotor induction machines are mechanically and electrically coupled. Mechanical coupling is achived either directly or through gears, while connecting the rotor circuits provides the electric coupling. The method was launched in 1893 by Steimmetz and Gorge [2]. The idea of obtaining a single unit was implemented by Hunt in 1907 [2]. The Hunt motor represented a considerable advance over earlier machines, in that it comprised a single rotor with two stator windings sharing a common magnetic circuit.

The mixed pole machine presented in this paper comprises two stator windings with different number of pole pairs, namely P_1 and P_2, and reluctance rotor with $P_r = P_1+P_2$ saliencies, as shown in fig. 1. The two fields produced by the two-stator windings share the same magnetic circuit. This machine is to be studied when operating in the generation mode.

This paper presents a novel modeling technique that is suitable for generation mode. This method assumes that the machine is current fed through the control winding. The MMF distribution through the rotor periphery is obtained. Hence, the flux density distribution is also calculated by numerical integration of the flux density. This method handles the machine harmonics due to rotor saliencies and discusses the effect of skewing on the output voltage harmonics.

The paper also discusses the effect of different excitation conditions the shape of the total MMF.

Moreover, it presents the simulation study of MPM radial forces and the effect of unsymmetrical distribution of the machine flux on the resultant radial force. All calculations are based on the proposed model that uses the machine magnetic circuit. The effect of winding frequency, MMF magnitude and relative phase shift on the total MMF wave is also considered.

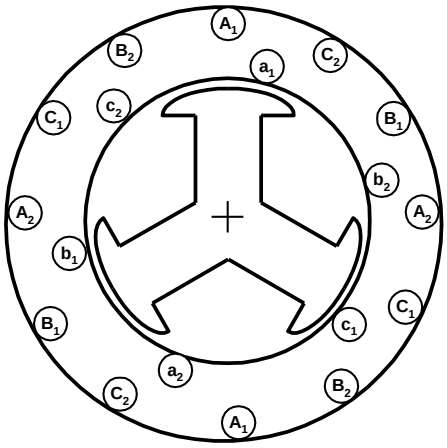

Fig. 1. 4/2 poles MPM with reluctance rotor.

2. The proposed simulation model

The actual magnetic circuit is used to model the proposed machine so as to account for the field space harmonics resulted from the rotor saliencies. Fig. 2 shows the MMF distribution in the space, *F (Φ)*, when the 2-pole winding is fed from a dc supply and the 4-pole winding is open circuited.

Fig. 3 illustrates the inverse air gap function of the three saliencies skewed rotor and fig. 4 illustrates the air gap flux density.

The air gap flux density distribution, *B(Φ)*, is given by [4]:

$$B(\phi) = \mu_o g^{-1}(\phi) F(\phi) \quad . \tag{1}$$

Where $g^{-1}(\Phi)$ is the inverse air gap function.

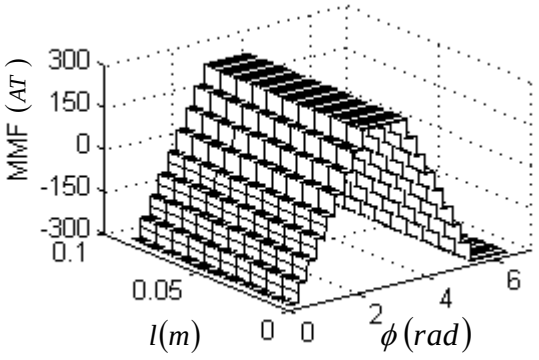

Fig. 2. Total MMF.

The flux linking each phase is obtained by numerical integration of the flux density under the coil span. It should be noted that the coil span varies according to the number of poles of each stator winding. The flux linking each phase is then differentiated to obtain the corresponding phase voltage. A MATLAB S-function is written to simulate the MPM using the above-mentioned method. In this method, the effects of saturation as well as that of slot harmonics are neglected.

3. Radial force

Magnetic radial forces are produced in all types of electrical machines due to the radial component of the distributed air gap flux. In machines with symmetrical winding and constant air gap, the resultant of these distributed radial forces balance out with near

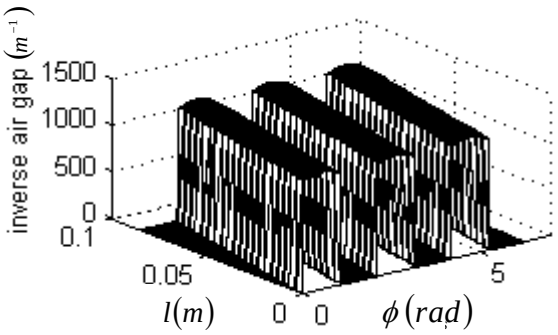

Fig. 3, Inverse air gap function

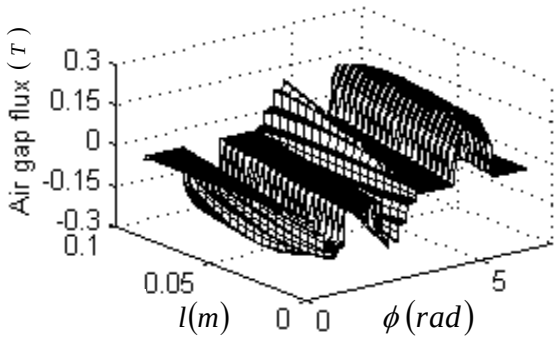

Fig. 4. Air gap flux density.

zero value. The air gap irregularity or windings asymmetry will give rise to unbalanced magnetic pull. In practice, unbalanced magnetic pull is an undesirable feature and must be avoided to reduce accompanying noise, vibrations and other undesirable effects such as current and torque harmonics. Conventional machines are usually designed to avoid such unbalance in magnetic pull. In mixed pole machines with a stator of two symmetrical poly phase sets of windings and constant air gap, the air gap radial force distribution depends on the combinations of the two stator pole pair numbers P_1 and P_2.

As will be shown, when P_1-P_2 = 1, the resultant magnetic radial force will not be zero for both concentric and eccentric rotors [1]. In this case the direction of the resultant radial force is determined by the frequencies of the two windings ω_1 and ω_2. For equal frequencies $\omega_1 = \omega_2$, the resultant radial force is stationary, and the direction of this stationary force is determine by the phase difference between the currents of the two stator winding.

The specific field energy method is used to calculate the MPM radial force. This method is suitable for machines with different air gap configuration. The air gap may be constant or variable, i.e. the rotor may be cylindrical or salient, concentric or eccentric. The method is based on the well-known formula of force attraction F between infinitely permeable ferromagnetic surfaces with flux density B_g crossing the air gap surface area A between them. The air gap flux density B_g is given by eq. (1).

For an infinitesimal small air-gap area dA the radial force is given by:

$$dF = \frac{B_g^{\,2}}{2\mu_o}\, dA \cdot \tag{2}$$

Where,

$$dA = R \cdot l \cdot d\phi \,,$$

and the horizontal and vertical radial force components dF_x and dF_y are estimated from:

$$dF_x = \frac{B_g^{\,2}}{2\mu_o} \cos(\phi) \cdot dA, \tag{3}$$

$$dF_y = \frac{B_g^{\,2}}{2\mu_o} \sin(\phi) \cdot dA \cdot \tag{4}$$

The radial force components F_x and F_y are then calculated by the integration over the total air gap surface $(0 \le \phi \le 2\pi)$.

$$F_x = \int_0^{2\pi} \frac{B_g^{\,2}}{2\mu_o} \cos(\varphi) \cdot dA \tag{5}$$

$$F_y = \int_0^{2\pi} \frac{B_g^{\,2}}{2\mu_o} \sin(\phi) \cdot dA \tag{6}$$

3.1. Stator MMF of mixed pole machine

Assuming that the fields produced by the two stator windings are sinusoidally distributed and given by:

$$F_1(\phi, t) = F_{m1} \cos(\omega_1 t - P_1 \phi - \alpha_1) \,, \tag{7}$$

$$F_2(\phi, t) = F_{m2} \cos(\omega_2 t - P_2 \phi - \alpha_2) \,, \tag{8}$$

where

ϕ	is the mechanical stator space angle measured from the reference (phase A) of stator 1,
P_1 and P_2	are the pole pair numbers of the two windings,
$\omega_1$and ω_2	are is the excitation frequencies of the two windings,
α_1 and α_2	are is the phase shift of MMFs of the two stator windings at time zero, and
F_{m1} and F_{m2}	are is the MMF amplitudes of the two stator windings.

Let $F_{m2} = k\, F_{m1}$.

The stator total MMF is the sum of the two space phasors, as shown in fig. 5, and it is given by:

$$\bar{F} = \bar{F_1} + \bar{F_2} \,. \tag{9}$$

Hence, the total MMF can be written in complex form as:

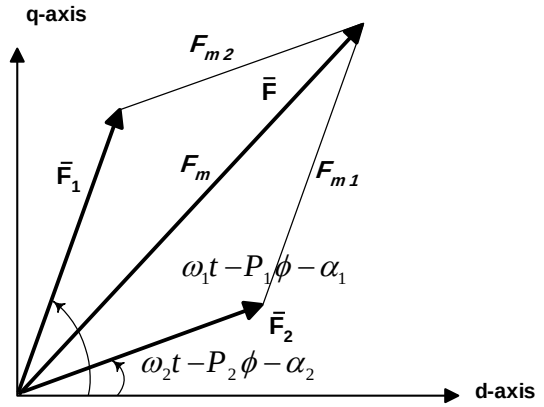

Fig. 5. Stator MMF.

$$\bar{F} = F_m e^{j\theta}, \tag{10}$$

where,

$$F_m = \sqrt{F_{m1}^2 + (kF_{m1})^2 + 2kF_{m1}^2 \cos((\omega_1 - \omega_2)\cdot t - (P_1 - P_2)\cdot\phi - (\alpha_1 - \alpha_2))}, \tag{11}$$

$$\theta = \sin^{-1}\left(\frac{F_{m1}}{F_m}\cdot \sin((\omega_1 - \omega_2)\cdot t - (P_1 - P_2)\cdot\phi - (\alpha_1 - \alpha_2))\right) + \omega_2 t - P_2\phi - \alpha_2 \tag{12}$$

Eq. (12) states that the stator total MMF is a space phasor with variable magnitude F_m and variable phase θ. Also, the envelope of the total MMF is described by the peaks of the total MMF patterns, which is given by eq. (12).

For $P_1 - P_2 = 1$ and (ω_1=ω_2), eq. (12) dictates that the envelope of the MMF wave will be stationary and it is reduced to:

$$F_m = \sqrt{F_{m1}^2 + (kF_{m1})^2 + 2kF_{m1}^2 \cos(\phi + (\alpha_1 - \alpha_2))}\ . \tag{13}$$

In the following, the effect of different magnitude, different excitation frequencies, and different phase shift is thoroughly investigated with illustrative figures for the considered 4/2 poles MPM.

3.1.1. Effect of windings frequencies

The effect of winding frequencies is discussed according to the following cases. The first case, when the two windings are excited with same frequency of 50Hz and same phase sequence (i.e. $\omega_1 = \omega_2$). The MMF distribution is illustrated in fig. 6 for four time instants ($t = 0, \pi/4\omega_1, \pi/2\omega_1, 3\pi/4\omega_1$) while the two stator MMF have the same magnitude. Since the frequencies of the two windings are equal, the envelope is stationary. The mixed pole wave will rotate CCW with speed $(\omega_1+\omega_2)/(P_1+P_2)$ = 209.3 rad/sec [1]:

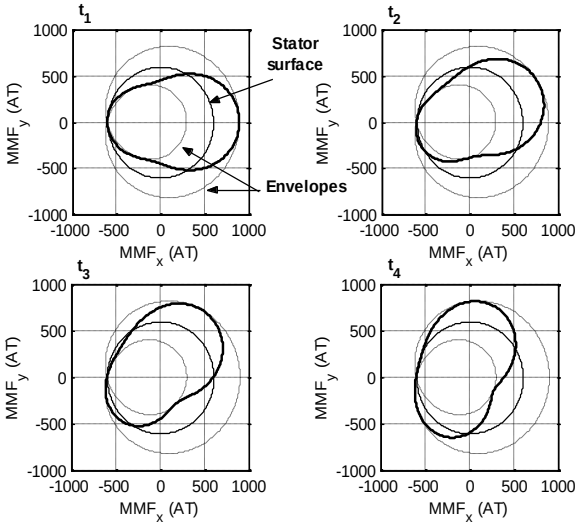

Fig. 6. Same frequency and same sequence.

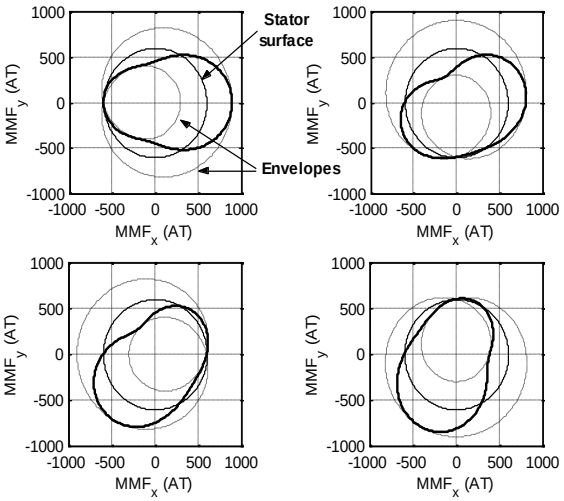

Fig. 7. Same frequency and same sequence.

The second case, when the two windings are excited with the same frequency of 50Hz but reversed phase sequence (i.e. $\omega_1 = -\omega_2$). The MMF distribution is illustrated in fig. 7 for the same four time instants ($t = 0, \pi/4\omega_1, \pi/2\omega_1, 3\pi/4\omega_1$), while the two stator MMF have also the same magnitude. Since the frequencies of the two windings are equal, the envelope rotates with speed of. $(\omega_1-\omega_2)/(P_1-P_2)$ = 628 rad/sec while the synchronous speed will be zero.

3.1.2. Effect of phase shift ($a = a_1 - a_2$)

In this case, the two windings are excited with the same frequency and same phase sequence such that the MMF envelope is stationary. The MMF distribution is illustrated in fig. 8 for different values of a ($0, \pi/4, \pi/2, 3\pi/4$) while the two stator MMF have also the same magnitude. The envelope stationary axis direction is is shown to be determined by the phase shift (a_1-a_2). This angle can be controlled by controlling the current in one or both of the stator windings and the desired direction can be obtained.

3.1.3. Effect of two stators MMF magnitude

In this case, the two windings are excited with the same frequency and same phase sequence such that the MMF envelope is stationary. The MMF distribution is illustrated in fig. 9 for different values of k (0, 1/3, 2/3, 1). For small k, the stator total MMF is similar

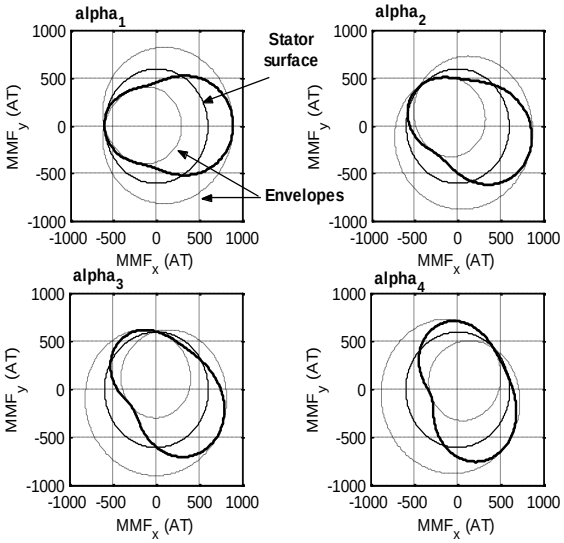

Fig. 8. Effect of phase angle a.

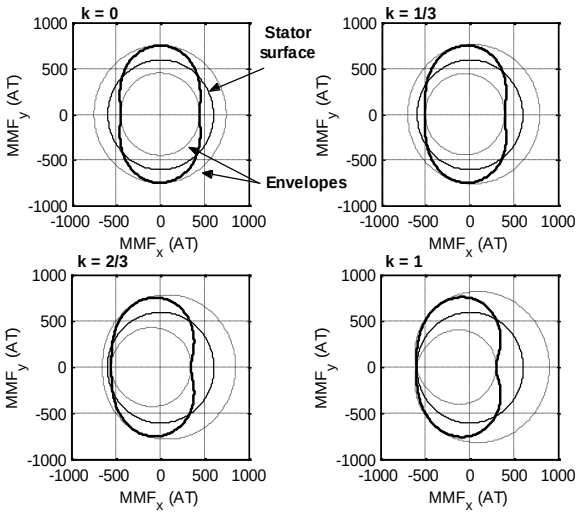

Fig. 9. Effect of different two stators MMF magnitudes.

to that produced by 4-pole only. As k increases, the magnetic field has an equivalent P_1+P_2 pole. For the 4/2 poles MPM, the equivalent number of poles is odd. Fig. 9 shows that for k =1, the rotor field has two north poles and one south pole at the specified time instant.

3.2. Air gap length

If the rotor is cylindrical, the air-gap length g_c between the rotor and the stator; with eccentric displacements are small enough compared to the rotor radius, can be written as [3]:

$$g_c = g_o - x\cos(\phi) + y\sin(\phi), \tag{14}$$

where g_o is the air-gap length when the rotor center is aligned to the stator center. x and y are the displacements in the two-quadrature axes. Then, the inverse gap function can be written as:

$$g_c^{-1}(\phi_s) = \frac{1}{g_o}\left(1 + \frac{x}{g_o}\cos(\phi) - \frac{y}{g_o}\sin(\phi)\right). \tag{15}$$

The inverse air gap function for concentric and eccentric salient rotor is shown in fig. 10.

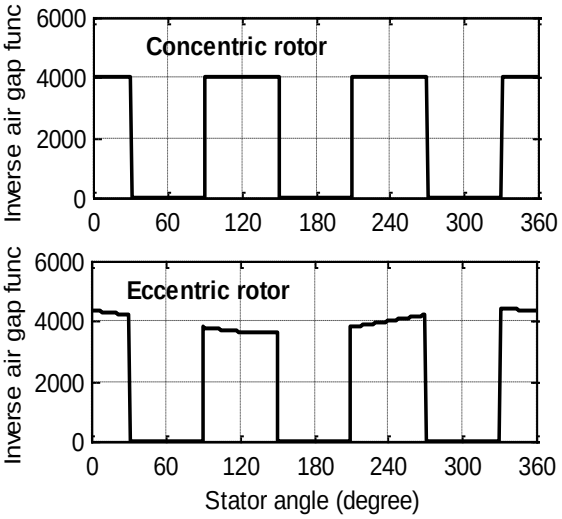

Fig. 10. Inverse air gap function for concentric and eccentric salient pole rotor.

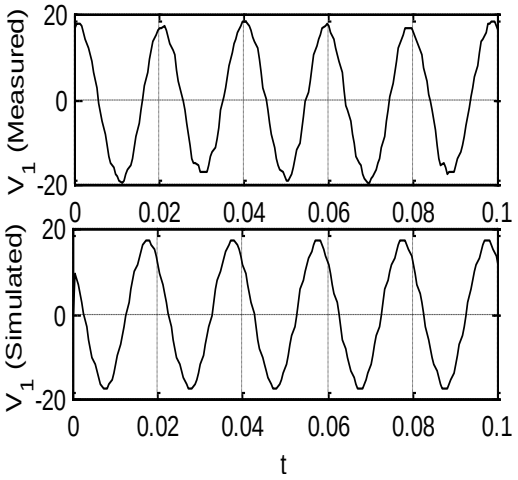

Fig. 11. Output voltage for DC excitation.

4. Simulation and experimental results

4.1. Machine output voltage

Comparison between measured and simulated output voltage is illustrated in fig. 11. The machine is driven at a constant speed of 1000 rpm, with dc excitation applied to the 2-pole winding. Hence the output frequency is found to be 50 Hz according to the following eq. [1]

$$\omega_m = \frac{\omega_1 + \omega_2}{P_1 + P_2}. \tag{16}$$

Figs. 12 and 13 illustrate the experimental results obtained when using a six pulse, 180° conduction, voltage source inverter. The inverter provides variable frequency and variable voltage magnitude excitation. Fig. 12 illustrates the experimental waveforms when the 2-pole winding is excited at 15 Hz and 100% duty cycle. The output frequency is found to be 65 Hz as shown in fig. 13. The simulated output voltage shown in fig. 13 is found to adequately match the experimental results. To change the voltage magnitude, the duty cycle is changed as shown in figs. 14 and 15.

The effect of skewing the rotor saliencies on the generated voltage induced harmonics is

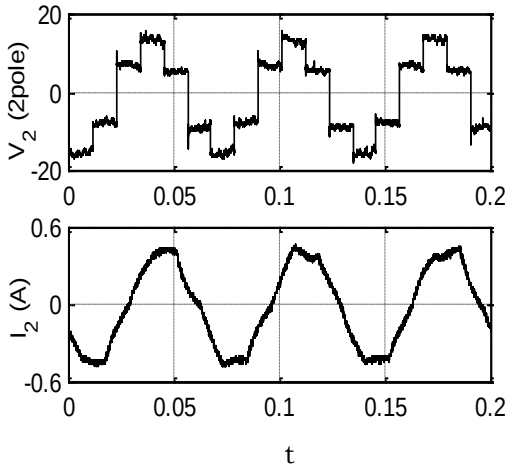

Fig. 12. Measured phase voltage and current of a 6-pulse inverter 180° conduction.

also considered. Fig. 16 illustrates the experimental and simulated waveforms for unskewed rotor when the machine is driven at a constant speed of 1000 rpm, with dc excitation applied to the 2-pole winding. The output frequency is found to be 50 Hz. Fig. 17 illustrates the experimental and simulated waveforms for skewed rotor operating at same conditions. It should be noted that the effect of skewing is to reduce the output voltage induced harmonics. Moreover, the rotor skewing reduces the mutual inductance between the two windings. Consequently, the output

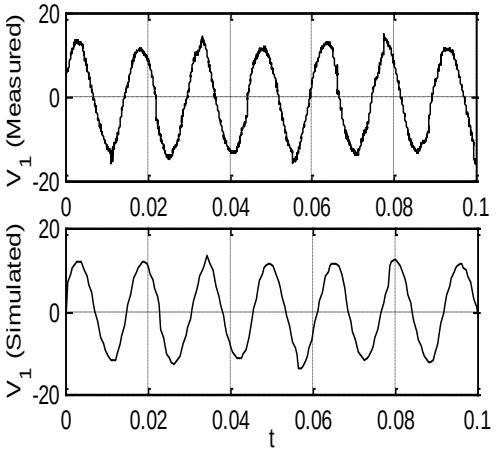

Fig. 13. Output voltage for AC excitation.

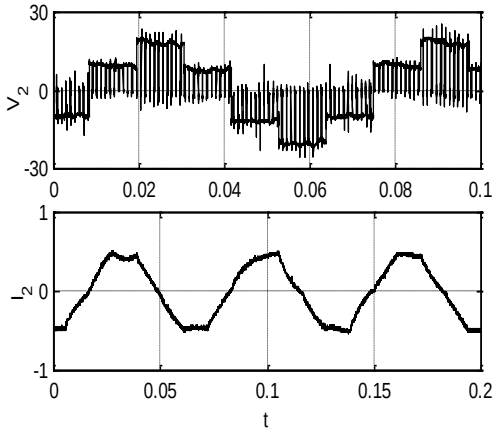

Fig. 14. Measured phase voltage and current of a 6-pulse inverter 180^{o} conduction.

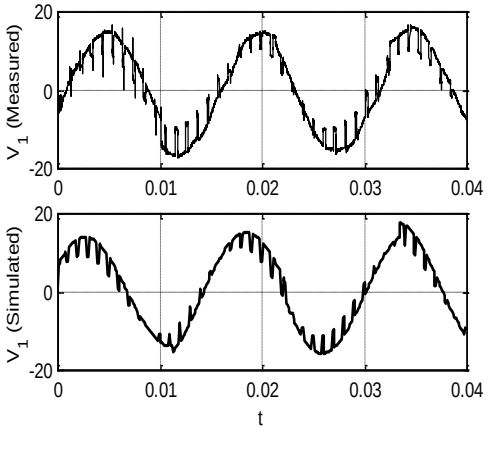

Fig. 15. Output voltage for AC excitation.

voltage magnitude is reduced. The simulated output voltage shown in fig. 17 is found to adequately match the experimental results. However, for unskewed rotor, the simulated output voltage shown in fig. 16 is found to be slightly mismatching the experimental results. This is due to neglecting the effect of slot harmonics.

4.2. Radial forces

The radial force is computed for different frequencies at different speeds to illustrate the profile of the radial force in *x-y* plane according to the following cases.

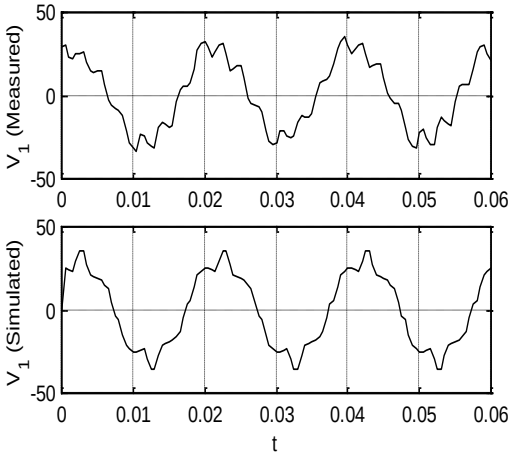

Fig. 16. Output voltage for unskewed rotor.

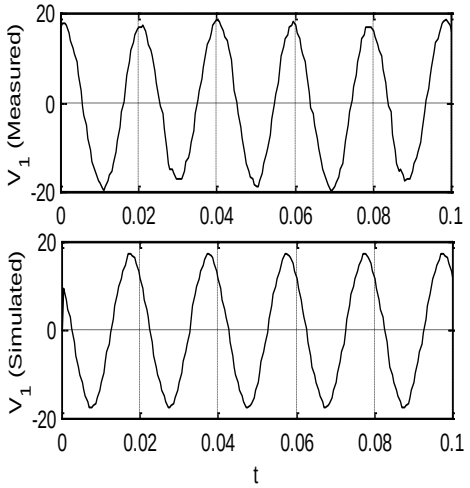

Fig. 17. Output voltage for skewed rotor.

4.2.1. Singly fed operation

In this case, only one winding is to be fed while the other one is open circuited. Two cases are considered. First case when the 4-pole winding is fed by a current of 1 A (peak value) at a frequency of 50 Hz. The radial force profile for two different speeds is shown in fig. 18. At 1000 r.p.m, the radial force magnitude is constant while its direction varies with time. When the machine speed is 2000 r.p.m ($\omega_m = 2\omega/P_r$) the resultant radial force has the same constant magnitude with a constant direction.

When the 2-pole winding is fed with the same current while the 4-pole winding is open circuited, same results are obtained as shown in fig. 19.

4.2.2. Doubly fed operation

In this case, the machine is doubly fed. Diversity of cases are considered to illustrate the effect of eccentric displacement on the radial force profile as well as the effect of current sequence. In all cases the two windings are fed with the same current magnitude (1A peak value) and the same frequency of 50 Hz. The corresponding synchronous speed is given by eqn. (16).

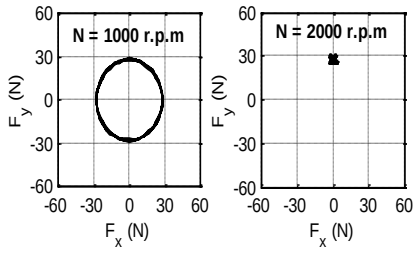

Fig. 18. Radial forces for single fed operation.

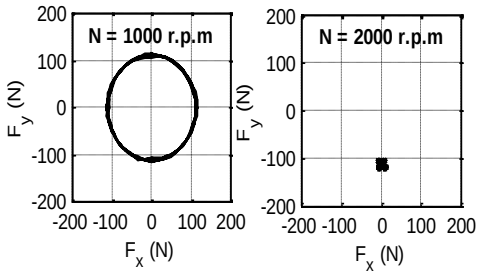

Fig. 19. Radial forces for single fed operation.

4.2.1.1. Same phase sequence with concentric rotor: In this case, the two winding currents have the same sequence and the rotor is positioned at the stator center. The radial forces profile at different phase shift between the winding currents is shown in fig. 20. The radial force has a constant magnitude at a fixed direction. The direction is determined by the relative phase shift between the winding currents.

Fig. 21 shows the radial force profile when the machine runs asynchronous speed. The resultant radial force magnitude profile is an eccentric elapse. The center of this elapse depends on the relative phase shift between the two winding currents.

4.2.1.2. Same phase sequence with eccentric rotor: In this case, it is assumed that the rotor is shifted from the stator center by a displacement of $0.2g_o$ in the x-direction. As in the previous case, the two winding currents are assumed to be equal and the machine runs at the synchronous speed of 2000 r.p.m. The radial force profile is shown in fig. 22. The resultant radial force magnitude profile has an eccentric shape due to the resultant harmonics. The center of each shape depends also on the relative phase shift between the two winding currents.

4.2.1.3. Reversed phase sequence with concentric rotor: In this case, the two windings currents have an opposite sequence, and the rotor is positioned to the stator center. The

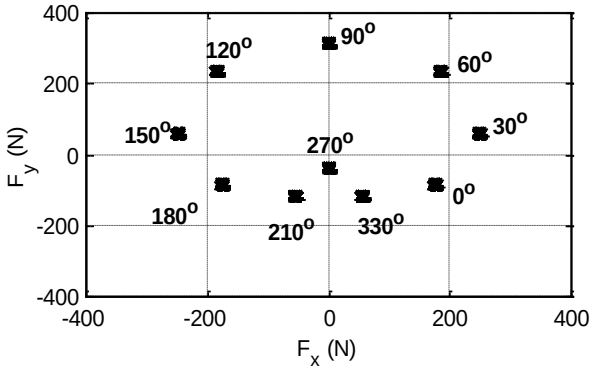

Fig. 20. Radial force profile for same sequence at elected phase shifts between winding currents when the machine runs at synchronous speed.

machine synchronous speed for euqal and opposite frequencies is zero, refer to eqn. 16. The radial force profile at different phase shift between the winding currents is shown in fig. 23. The radial force profile is a circle centered at the origin. The radius of the circle is determined by the relative phase shift between the winding currents.

4.2.1.2. Reversed phase sequence with eccentric rotor: In this case, it is assumed that the rotor is shifted from the stator center by a displacement of $0.2g_o$ in the x-direction. The machine speed is zero. The radial force profiles at different phase shift between the winding currents are shown in fig. 24. The radial force profile has an elliptic shape.

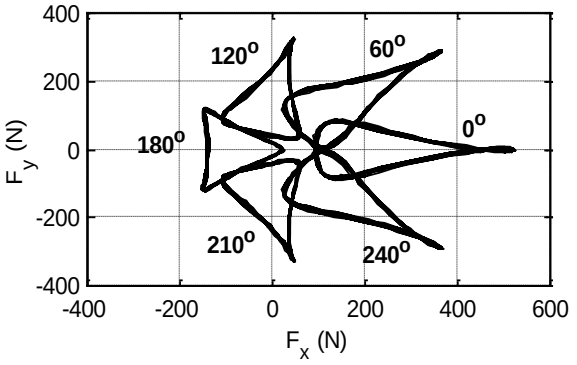

Fig. 22. Radial force profile for same sequence and with eccentric rotor.

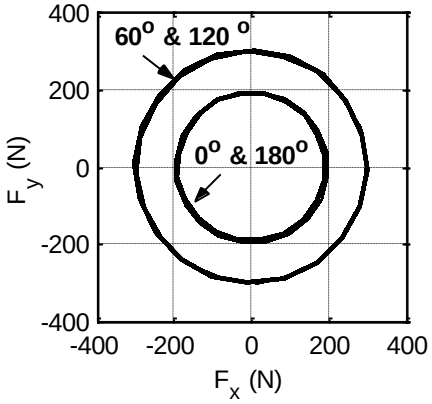

Fig. 23. Radial force profile for opposite sequence and concentric rotor.

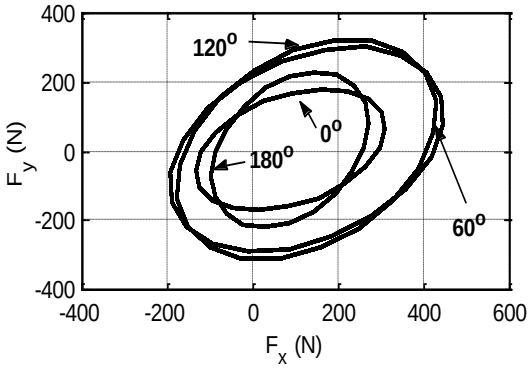

Fig. 24. Radial force profile for same sequence and with eccentric rotor.

5. Conclusions

In this paper, a novel modeling technique to MPM was presented. A reasonably good agreement was obtained between simulated and experimental values of the output machine voltage.

Also, a study to machine radial forces for concentric and eccentric rotors at different speeds was carried out. The total stator MMF was illustrated for different excitation conditions.

Appendix A

MPM machine data:
Rated power, 250 Watt
4-pole winding:
Rated voltage, 60 V
Rated current, 2.1 A
Rated frequency, 50 Hz
2-pole winding:
Control voltage, 0 to 120 V
Rated current, 1.2 A
Control frequency, -50 to 50 Hz
Number of turns per phase per pole
2-pole winding, 140 turn
4-pole winding, 70 turn
Machine Dimensions:
Rotor radius, 3 cm
Rotor length, 8.5 cm
Air gap length, 0.375 mm
Machine Parameters:
4-pole stator: $R_1 = 22.3\ \Omega$, $L_1 = 0.1084$ H
2-pole stator: $R_2 = 23.43\ \Omega$, $L_2 = 0.4072$ H
Mutual Inductance between two stators: $M_{12} = 0.115$ H

References

[1] M. Mustafa El_Daba, Mixed Pole Machine, Ph.D Thesis, Alexandria University, Egypt (2001).

[2] R. W. Broadway, L. Burbridge, Self-Cascaded Machine: a Low-Speed Motor or High-Frequency Brushless Alternator, PROC., IEE, Vol. 117 (7), pp. 1277-1290 (1970).

[3] T. Chiba, T. Deido, NTD Fukao and M.A. Rahman, "An Analysis Of Bearingless ac Motors", IEEE Trans on Energy Conversion, Vol. 9 (1), pp. 61-67 (1994).

[4] A. Chiba, M.A. Rahman and Tadashi Fuako, "Radial Force in a Bearingless Reluctance Motor", IEEE Trans on Magnetics, Vol. 27 (2), pp. 786-790 (1991).

[5] L. Xu, F. Liang and T.A. Lipo, "Transient Model of a Doubly Excited Reluctance Motor", IEEE Trans on Energy Conversion, Vol. 6 (1), pp. 126-133 (1991).

Received May 11, 2004
Accepted June 20, 2004